Inorganic Chemistry

Article

pubs.acs.org/IC

Voltammetric Determination of the Reversible Potentials for $[\{Ru_4O_4(OH)_2(H_2O)_4\}(\gamma\text{-}SiW_{10}O_{36})_2]^{10-}$ over the pH Range of 2−12: Electrolyte Dependence and Implications for Water Oxidation Catalysis

Yuping Liu, Si-Xuan Guo, Alan M. Bond,* and Jie Zhang*

School of Chemistry, Monash University, Clayton, Victoria 3800 Australia

Yurii V. Geletii* and Craig L. Hill

Department of Chemistry, Emory University, 1525 Dickey Drive, Atlanta, Georgia 30322, United States

Supporting Information

ABSTRACT: Voltammetric studies of the Ru-containing polyoxometalate water oxidation molecular catalyst $[\{Ru_4O_4(OH)_2(H_2O)_4\}(\gamma\text{-}SiW_{10}O_{36})_2]^{10-}$ ($[\mathbf{1}(\gamma\text{-}SiW_{10}O_{36})_2]^{10-}$ where **1** represents the $\{Ru_4O_4(OH)_2(H_2O)_4\}$ core and **1**(0) stands for its initial form with all ruthenium centers in the oxidation state IV) have been carried out in aqueous media over a wide range of pH (2−12 using Britton−Robinson buffer) and ionic strength. Well-defined voltammograms in buffered media are only obtained when Frumkin double layer effects are suppressed by the presence of a sufficient concentration of additional supporting electrolyte ($LiNO_3$, $NaNO_3$, KNO_3, $Ca(NO_3)_2$, $Mg(NO_3)_2$, $MgSO_4$, or Na_2SO_4). A combination of data derived from dc cyclic, rotating disk electrode, and Fourier transformed large amplitude ac voltammetry allow the assignment of two processes related to reduction of the framework and the complete series of $Ru^{III/IV}$ and $Ru^{IV/V}$ redox processes and also provide their reversible potentials. Analysis of these data reveals that K^+ has a significantly stronger interaction with **1**(1) (the number inside bracket stands for the number of electrons removed from **1**(0)) than found for the other cations investigated, and hence its presence significantly alters the pH dependence of the **1**(0)/**1**(1) reversible potential. Comparison of experimental data with theory developed in terms of equilibrium constants for process **1**(0)/**1**(1) reveals that both H^+ and K^+ interact competitively with both **1**(0) and **1**(1). Importantly, reversible potential data reveal that (i) proton transfer does not necessarily need to be coupled to all electron transfer steps to achieve catalytic oxidation of water, (ii) the four-electron oxidized form, **1**(4), is capable of oxidizing water under all conditions studied, and (iii) under some conditions, the three-electron oxidized form, **1**(3), also exhibits considerable catalytic activity.

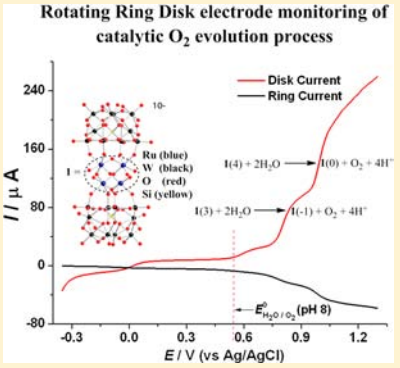

INTRODUCTION

Polyoxometalates (POMs) are of substantial fundamental and applied interest. For example, many are excellent molecular catalysts for a wide range of reactions in either the presence or absence of light.[1,2] POMs are highly stable over a range of redox levels, and their redox and catalytic properties can be tuned by changing the heteroatoms without affecting their gross structures.[3,4] Furthermore, some lacunary POMs can be used as ligands to stabilize the catalytically active oxide cores, creating additional structural diversity in their use as molecular catalysts.[5,6]

Of relevance to this work, it has been shown that Ru- or Co-containing POM molecular catalysts may exhibit excellent catalytic activity with respect to the water oxidation reaction, which generates O_2 and H^+ ($2H_2O \rightarrow 4H^+ + O_2 + 4e^-$).[5,7−11] At the same time, it has been shown that the hydrolytic stability of $[Co_4(H_2O)_2(PW_9O_{34})_2]^{10-}$ under electrochemical catalytic water oxidation conditions is strongly dependent on experimental conditions.[12−14] $[\{Ru_4O_4(OH)_2(H_2O)_4\}(\gamma\text{-}SiW_{10}O_{36})_2]^{10-}$ ($[\mathbf{1}(\gamma\text{-}SiW_{10}O_{36})_2]^{10-}$ where **1** represents the $\{Ru_4O_4(OH)_2(H_2O)_4\}$ core), first synthesized by the Hill[7] and Bonchio[5] groups, is one of the most stable POM water oxidation catalysts reported so far. In this compound, the four ruthenium centers span a slightly distorted tetrahedron and are stabilized by hydroxo and oxo ligands (see Figure 1 for the structure). Geletii et al.[7] have used $[\mathbf{1}(\gamma\text{-}SiW_{10}O_{36})_2]^{10-}$ as a homogeneous catalyst and $[Ru(bpy)_3]^{3+}$ (bpy = tris(2,2′-bipyridyl)) as the oxidant for catalytic water oxidation reaction at pH 7. They reported that the reaction follows a complex mechanism that involves multiple intermediates. A turnover number of 18 (mol O_2/mol $[\mathbf{1}(\gamma\text{-}SiW_{10}O_{36})_2]^{10-}$) and turnover frequency (TOF) ≈ 0.5 s^{-1} were achieved.[7,15] Sartorel et al.[5] used Ce^{4+} as the oxidant at pH = 0.6. A TOF of 0.13 s^{-1} was

Received: July 8, 2013
Published: October 8, 2013

   dx.doi.org/10.1021/ic401748y | *Inorg. Chem.* 2013, 52, 11986−11996

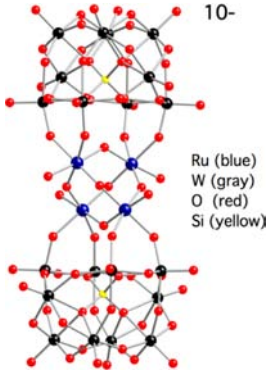

Figure 1. The structure of $[\mathbf{1}(\gamma\text{-}SiW_{10}O_{36})_2]^{10-}$.

reported under these conditions, and a TOF of ~280 s^{-1} was estimated at neutral pH.[16]

$[\mathbf{1}(\gamma\text{-}SiW_{10}O_{36})_2]^{10-}$ has also been immobilized onto carbon based electrode materials and used as a heterogeneous catalyst for water oxidation. Toma et al.[17] immobilized $[\mathbf{1}(\gamma\text{-}SiW_{10}O_{36})_2]^{10-}$ onto multiwalled carbon nanotubes functionalized with positively charged polyamidoamine ammonium (PAMAM) dendrimers for highly efficient electrocatalytic water oxidation. At pH 7, a TOF of 0.028 s^{-1} was observed at an overpotential of 0.48 V. A factor ca. 2 improvement has been achieved by the same research groups when multiwalled carbon nanotubes were replaced with graphene.[18] However, even though multiwalled carbon nanotubes and graphene are electrical conductors, PAMAM is nonconductive, which introduces an additional barrier to electron transfer. Therefore, it can be expected that the presence of PAMAM may also affect the catalytic performance of $[\mathbf{1}(\gamma\text{-}SiW_{10}O_{36})_2]^{10-}$. In order to overcome this drawback, we have confined $[\mathbf{1}(\gamma\text{-}SiW_{10}O_{36})_2]^{10-}$ within a highly porous and conductive graphene film to form stable modified electrodes. These $[\mathbf{1}(\gamma\text{-}SiW_{10}O_{36})_2]^{10-}$–graphene modified electrodes show excellent catalytic activity and stability toward water oxidation reaction at pH 7.5 in the presence of 1 M $Ca(NO_3)_2$.[19] A TOF of 0.82 s^{-1} was observed at an overpotential of 0.35 V, which is almost 2 orders of magnitude higher than the PAMAM functionalized multiwalled carbon nanotube supported $[\mathbf{1}(\gamma\text{-}SiW_{10}O_{36})_2]^{10-}$. The feature that $[\mathbf{1}(\gamma\text{-}SiW_{10}O_{36})_2]^{10-}$ is directly in contact with graphene is postulated to be the reason for the improved catalytic activity.

It has been suggested that protons often play an important role in the water oxidation reaction catalyzed by molecular catalysts.[6,20,21] It has been pointed out that all four sequential one-electron oxidations of the "blue dimer" catalyst forming the active species may proceed via a proton-coupled electron transfer mechanism.[22] A similar mechanism was proposed for $[\mathbf{1}(\gamma\text{-}SiW_{10}O_{36})_2]^{10-}$ based on density functional theory calculations but without experimental evidence from the Pourbaix diagram.[23] It is also well-known that proton transfer is often coupled to POM electron transfer processes on the voltammetric time scale.[24,25] However, despite the fact that **1** exhibits a range of attractive properties for the catalytic water oxidation application, the detailed mechanisms, especially regarding the active forms of the catalyst and the role of proton under the catalytic turnover conditions remain controversial.[26] In principle, this could be resolved by the construction of a Pourbaix diagram over a wide pH range to show the pH dependence of reversible potentials of the redox processes associated with catalytically active Ru centers, since these diagrams provide information on the number of protons involved in each electron transfer step under different pH conditions. In a previous study,[27] we restricted our studies of the electrochemistry of $[\mathbf{1}(\gamma\text{-}SiW_{10}O_{36})_2]^{10-}$ to acidic media (pH = 1–3.8) where, unlike at higher pH, voltammograms are well-defined. Within this acidic pH range, the slopes of plots of reversible potential versus pH for the first two oxidation ($Ru^{IV/V}$) and first two reduction ($Ru^{IV/III}$) processes are 57 ± 6 mV, which is commonly interpreted as a reversible one-electron transfer reaction coupled with one proton transfer.[25,28,29] Although this study provides some useful information on the electrochemical properties of $[\mathbf{1}(\gamma\text{-}SiW_{10}O_{36})_2]^{10-}$ in acidic media, the data obtained do not provide direct insight into the mechanism of more efficient catalytic water oxidation carried out under both neutral and basic pH conditions.[30]

The complexity in the voltammetry of $[\mathbf{1}(\gamma\text{-}SiW_{10}O_{36})_2]^{10-}$ at pH > 4 is likely to be associated with the high negative charge. Our recent studies[19] have revealed that when the electrolyte concentration is ≤0.1 M (Debye length of ~1 nm or less), the voltammetry of $[\mathbf{1}(\gamma\text{-}SiW_{10}O_{36})_2]^{10-}$ suffers from a significant Frumkin effect[31−34] that can lead to a slower than expected electron transfer rate and provide substantial departure from ideal characteristics expected from simple reversible diffusion controlled behavior. Thus, observation of well-defined voltammograms of $[\mathbf{1}(\gamma\text{-}SiW_{10}O_{36})_2]^{10-}$ in pH 7 aqueous phosphate buffer solution required high ionic strength conditions (addition of 1 M supporting electrolyte) to suppress Frumkin double layer effects by decreasing both the double layer thickness and the effective charge of $[\mathbf{1}(\gamma\text{-}SiW_{10}O_{36})_2]^{10-}$. On this basis, high electrolyte concentration is also therefore generally to be required to achieve well-defined current–potential curves in neutral and alkaline conditions.

In this study, the electrochemistry of $[\mathbf{1}(\gamma\text{-}SiW_{10}O_{36})_2]^{10-}$ has been investigated using dc cyclic, rotating (ring) disk electrode, and the sophisticated Fourier transformed large amplitude alternating current voltammetry (FTAC voltammetry)[35] under a wide range of conditions. In particular, the pH, ionic strength, and type of supporting electrolyte have been varied systematically to establish the acid–base and ion-paring properties in different redox states, to identify the active forms of the catalyst, and to determine the role of protons and cations on catalytic water oxidation. With respect to variation of pH, Britton–Robinson (BR) buffer was chosen since it allows a very wide pH range from 2 to 12 to be studied with just one buffer system.[36]

EXPERIMENTAL SECTION

Reagents. $Rb_8K_2[\mathbf{1}(\gamma\text{-}SiW_{10}O_{36})_2]$ was synthesized using procedures described elsewhere.[30] Ferrocenemethanol (FcMeOH, 97%), KNO_3, $NaNO_3$, $LiNO_3$, and $Ca(NO_3)_2$ (AR grade, BDH) and H_3PO_4, H_3BO_3, and acetic acid (AR grade, Univar) were used as supplied by the manufacturers. Deionized water from a Milli-Q-MilliRho purification system (resistivity 18 MΩ cm) was used to prepare all aqueous electrolyte solutions. BR buffer solutions having the desired pH values were prepared from a solution containing 0.040 M each of H_3PO_4, H_3BO_3, and acetic acid with adjustment of pH by the addition of 0.2 M NaOH to solutions having higher acidity. pH values were determined with a Hannah HI 8314 membrane pH meter (Hannah, Ltd.) and a Hannah HI 1230 combination electrode.

Electrochemistry. Conventional dc cyclic voltammetric and rotating disk electrode experiments were carried out using a CHI 700D electrochemical workstation (CH Instruments, Austin, Texas, USA). A rotating disk electrode rotator (RRDE-3A) (ALS, Japan) connected to the CHI 700D electrochemical workstation was used for

dx.doi.org/10.1021/ic401748y | Inorg. Chem. 2013, 52, 11986–11996

both RDE and rotating ring disk electrode (RRDE) experiments. Large amplitude Fourier transform ac voltammetric measurements were undertaken with a home-built apparatus,[35] using an applied sine wave perturbation (amplitude 80 mV and frequency 9.02 Hz), superimposed onto the dc ramp. The total current measured by this waveform was then subjected to Fourier transformation to obtain a power spectrum. After selection of the frequency band of interest, inverse Fourier transformation is used to generate the required dc or ac harmonic components.[35]

All voltammograms were acquired at 22 ± 2 °C. A standard three-electrode electrochemical cell arrangement was employed using a glassy carbon (GC), Au, or Pt working electrode (3.0 mm diameter for GC, 2.0 mm diameter for Au or Pt, CH Instruments, Austin, Texas, USA), a Pt wire counter electrode, and Ag/AgCl (3 M NaCl) reference electrode (0.210 V vs SHE).[37] Prior to each series of experiments, the working electrode was polished using an aqueous 0.3 μm alumina suspension on a polishing cloth (Buehler), rinsed with water, and then sonicated to remove excess alumina, before a final rinse with water. Before each measurement, the solution was purged with nitrogen for at least 3 min to remove O_2 and then maintained under a slightly positive pressure of nitrogen for the duration of the measurement. The initial potential for the transient cyclic voltammetric measurement was chosen to be the open circuit potential.

Theoretical Considerations. In principle, $[\mathbf{1}(\gamma\text{-}SiW_{10}O_{36})_2]^{10-}$, at each redox level, can associate with either the electrolyte cation (or cations) or a proton in a competitive manner (not necessarily the same site) as described by a ladder reaction scheme (Scheme 1, where the

Scheme 1. A Simplified Reaction Scheme That Describes the Reactions That Occur during a Voltammetric Experiment When Electroactive Species A Is Reduced to B in the Presence of a Proton Source and a Metal Cation That Both Interact with A and B

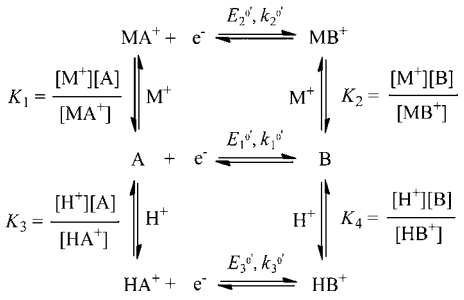

symbol A is used to represent $[\mathbf{1}(\gamma\text{-}SiW_{10}O_{36})_2]^{10-}$) and B its one electron reduced form (analogous arguments of course apply to an oxidation process). $[\mathbf{1}(\gamma\text{-}SiW_{10}O_{36})_2]^{10-}$, while written in this form for convenience, is unlikely to exist as an isolated 10 minus charged anion in aqueous electrolyte solution and at a minimum will be ion paired with an electrolyte cation or protonated by hydrolysis of water to lower the charge. As we have shown previously,[27] at high electrolyte concentration, 2−3 cations are always present in close proximity to the POM surface forming solvent separated ion pairs. Such an ion-pairing scenario does not obey a mass-action reaction rate law. Therefore, in Scheme 1, A and B are already ion-paired. Further ion-pairing, which obeys a mass-action reaction rate law, is considered in Scheme 1. If all electron transfer processes are well-separated, each can be treated individually.[38] In this scheme, $E_i^{0'}$ and $k_i^{0'}$ (i = 1, 2, and 3) stand for the formal potential and formal electron transfer rate constants, respectively, for the relevant heterogeneous charge transfer reaction, the charge transfer coefficient α is assumed to be 0.5, and Butler−Volmer kinetics are employed. Both metal cation interaction (ion-pair or complex formation) and protonation are expected to affect the characteristics of the voltammetry. If (a) both the electrolyte cation, M^+, and proton, H^+, compete for the same or each other's preferred binding site, (b) only a single interaction of the proton or metal ion occurs in each redox level, (c) all coupled homogeneous reactions are fully reversible on the voltammetric time scale, which can occur under buffered conditions even at high pH where $[H^+]$ is low since A and B can acquire H^+ directly from undissociated weak acid in the buffer or from solvent water,[25] (d) both the pH (buffered) and $[M^+]$ (large concentration excess) are unaltered during the voltammetric experiment, and (e) the contribution from any cross redox reactions are neglected, then the voltammetric characteristics can be described using a simplified overall one-electron transfer reaction A′/B′ with an apparent formal potential ($E_{app}^{0'}$) and an apparent standard electron transfer rate constant ($k_{app}^{0'}$), given in Scheme 2.

Scheme 2. A Simplified Reaction Scheme That Describes the Overall Reaction That Occurs during a Voltammetric Experiment When Electroactive Species A′ Is Reduced to B′ in the Presence of a Proton Source and a Metal Cation That Both Interact with A′ and B′

The $E_{app}^{0'}$ and $k_{app}^{0'}$ values are affected by the heterogeneous electron transfer reactions and also are functions of equilibrium constants of all coupled homogeneous reactions, pH and $[M^+]$. Their mathematical relationships (eqs 1−4) can be derived in the same manner as those used previously for simpler but related square reaction schemes.[25,39]

$$E_{app}^{0'} - E_1^{0'} = \frac{RT}{F}\ln\frac{1 + \frac{[M^+]}{K_2} + \frac{[H^+]}{K_4}}{1 + \frac{[M^+]}{K_1} + \frac{[H^+]}{K_3}} = \frac{RT}{F}\ln\frac{1 + \frac{[M^+]}{K_2} + \frac{[H^+]}{K_4}}{1 + \left(\frac{[M^+]}{K_2}\right)\left(\frac{K_2}{K_1}\right) + \left(\frac{[H^+]}{K_4}\right)\left(\frac{K_4}{K_3}\right)} \quad (1)$$

$$E_{app}^{0'} - E_2^{0'} = \frac{RT}{F}\ln\frac{\frac{K_2}{[M^+]} + 1 + \frac{K_2[H^+]}{K_4[M^+]}}{\frac{K_1}{[M^+]} + 1 + \frac{K_1[H^+]}{K_3[M^+]}} \quad (2)$$

$$E_{app}^{0'} - E_3^{0'} = \frac{RT}{F}\ln\frac{\frac{K_4}{[H^+]} + \frac{K_4[M^+]}{K_2[H^+]} + 1}{\frac{K_3}{[H^+]} + \frac{K_3[M^+]}{K_1[H^+]} + 1} \quad (3)$$

$$k_{app}^{0'} = \frac{k_1^{0'} + k_2^{0'}\left(\frac{[M^+]}{K_2}\right)^{\alpha}\left(\frac{[M^+]}{K_1}\right)^{1-\alpha} + k_3^{0'}\left(\frac{[H^+]}{K_4}\right)^{\alpha}\left(\frac{[H^+]}{K_3}\right)^{1-\alpha}}{\left(1 + \frac{[M^+]}{K_2} + \frac{[H^+]}{K_4}\right)^{\alpha}\left(1 + \frac{[M^+]}{K_1} + \frac{[H^+]}{K_3}\right)^{1-\alpha}} \quad (4)$$

To obtain eq 4, it is assumed that all heterogeneous electron transfer reactions share the same electron transfer coefficient value (α = 0.5). If metal ion interaction is insignificant compared with protonation, eq 4 can be written as in eq 5,[25]

$$k_{app}^{0'} = \frac{k_1^{0'} + k_3^{0'}\left(\frac{[H^+]}{K_4}\right)^{\alpha}\left(\frac{[H^+]}{K_3}\right)^{1-\alpha}}{\left(1 + \frac{[H^+]}{K_4}\right)^{\alpha}\left(1 + \frac{[H^+]}{K_3}\right)^{1-\alpha}} \quad (5)$$

The effect of K_4/K_3 (relative basicity of a POM in two redox levels) on $E_{app}^{0'}$ as a function of pH has been the subject of thorough investigation in cases where ion pairing is insignificant.[25] In this study, we need to establish the effect of both metal ion interaction and protonation on $E_{app}^{0'}$. The effects of pH on $E_{app}^{0'}$ for a range of (pM − pK_2) values (−6, −5, −4, −3, −2, −1, 0, 1) where pK and pM = −log K or −log M, respectively, were calculated using eq 1 when pK_2 − pK_1 = pK_4 − pK_3 = 5 (Figure 2). For comparison, the effects of pH on $E_{app}^{0'}$ were also computed for the extreme cases where either protonation or metal ion interaction is dominant. For example, when pM − pK_2 =

dx.doi.org/10.1021/ic401748y | Inorg. Chem. 2013, 52, 11986−11996

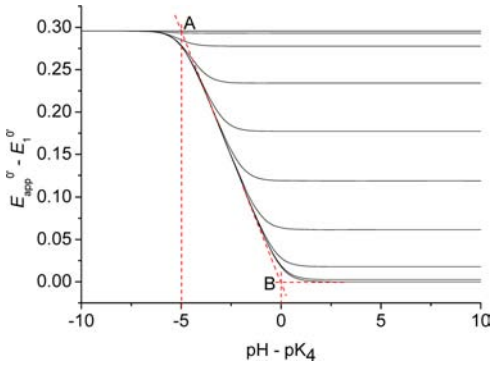

Figure 2. Dependence of $(E^{0'}_{app} - E^{0'}_{1})$ on $(pH - pK_4)$ as a function of $(pM - pK_2)$ calculated from eq 1 when $pK_2 - pK_1 = pK_4 - pK_3 = 5$. From top to bottom: $pM - pK_2 = -100, -6, -5, -4, -3, -2, -1, 0, 1, 100$.

100, protonation is dominant. It is well-known that if the difference between pK_3 and pK_4 is sufficiently large (i.e., >3), pK_3 and pK_4 values can be obtained separately from the transition points of the $(E^{0'}_{app} - E^{0'}_{1})$ vs $(pH - pK_4)$ curves (points A and B, Figure 2) when the effect of one of the protonation reactions is dominant.[38] As $pM - pK_2$ decreases, metal ion interaction plays an increasingly dominant role in the voltammetry (Scheme 1). Consequently, transition points of the $(E^{0'}_{app} - E^{0'}_{1})$ vs $(pH - pK_4)$ curves, which are commonly used to determine the pK_4 values, are now affected by metal ion interaction and can no longer be used to determine this value. As shown in Figure 2, these transition points shift to regions with smaller $(pH - pK_4)$ values as $pM - pK_2$ decreases. Eventually, and as expected, pH has no effect on $E^{0'}_{app}$ when metal ion interaction is dominant $(pM - pK_2 = -100)$. To compute the data shown in Figure 2, the same value of 5 was assigned to both $pK_2 - pK_1$ and $pK_4 - pK_3$. Since the interactions are at least partially electrostatic in nature and the reduced form is more negatively charged, the lower redox level is expected to interact more strongly with both the electrolyte cation and the proton. Importantly, as shown in Figure S1, Supporting Information, the validity of the conclusions given above remains when different values of $pK_2 - pK_1$ are used. The results in Figure 2 and Figure S1, Supporting Information, imply that in principle, pK_3 and pK_4 values can be determined using an electrolyte containing innocent cations following procedures described in our previous paper.[25] Subsequently, this information can be used to determine the pK_1 and pK_2 values of interactions involving noninnocent cations.

RESULTS AND DISCUSSION

Transient dc Cyclic and Steady-State RDE Voltammograms of $[1(\gamma\text{-}SiW_{10}O_{36})_2]^{10-}$ in BR Buffer in the Absence and Presence of KNO_3 as Additional Supporting Electrolyte. Cyclic voltammetric studies of $[1(\gamma\text{-}SiW_{10}O_{36})_2]^{10-}$ were undertaken in BR buffer solutions. At pH 2 (Figure 3a), eight well-defined processes, consisting of **1**(1)/**1**(2), **1**(0)/**1**(1), etc. associated with Ru centers and I/I′ and II/II′ associated with the W framework, were observed in the presence of 1 M KNO_3 supporting electrolyte. In the absence of 1 M KNO_3 (Figure 3a), not all processes are as well-defined, presumably due to the effect of electrical double layer on the highly negatively charged $[1(\gamma\text{-}SiW_{10}O_{36})_2]^{10-}$ as suggested previously.[19] Upon addition of 1 M KNO_3, these Frumkin effects are suppressed, and all processes are well-defined. Following nomenclature introduced in our previous study,[27] processes **1**(1)/**1**(2) and **1**(0)/**1**(1) are assigned to the one-electron oxidation of the Ru^{IV} centers, processes **1**(−1)/**1**(0), **1**(−2)/**1**(−1), **1**(−3)/**1**(−2), and **1**(−4)/**1**(−3) to the one-electron reduction of the Ru^{IV} centers, and processes I/I′ and II/II′ to the one-electron and four-electron reduction of W^{VI} centers, respectively. Reversible potential $(E^{0'})$ and peak separation (ΔE_p) data derived from cyclic voltammograms obtained in the presence of 1 M KNO_3 are summarized in Table 1. The reversible potentials were equated to the midpoint potential, which was derived from the average of the reduction and oxidation peak potentials $(E^{0'} = (E^{ox}_p + E^{red}_p)/2)$ and assuming the diffusion coefficients of both reduced and oxidized forms are equal. Since the influence of uncompensated resistance (ohmic IR_u effect) is minimal in aqueous media when a large concentration of KNO_3 is present, the fact that the ΔE_p $(E^{ox}_p - E^{red}_p)$ values for all seven one-electron processes are larger than the theoretical value of 56.5 mV predicted for a reversible one-electron transfer process at 25 °C implies that these processes are not fully electrochemically reversible.[31] This quasi-reversibility implies these processes could suffer from detectable Frumkin effects, which is enhanced when the electrolyte concentration is low (Figure 3a).[31] Cyclic voltammograms of $[1(\gamma\text{-}SiW_{10}O_{36})_2]^{10-}$ also show a small oxidation process (**1**(2)/**1**(3)), near the positive potential solvent limit. As in our previous studies,[19] this process is assigned to a third $Ru^{IV/V}$ process.

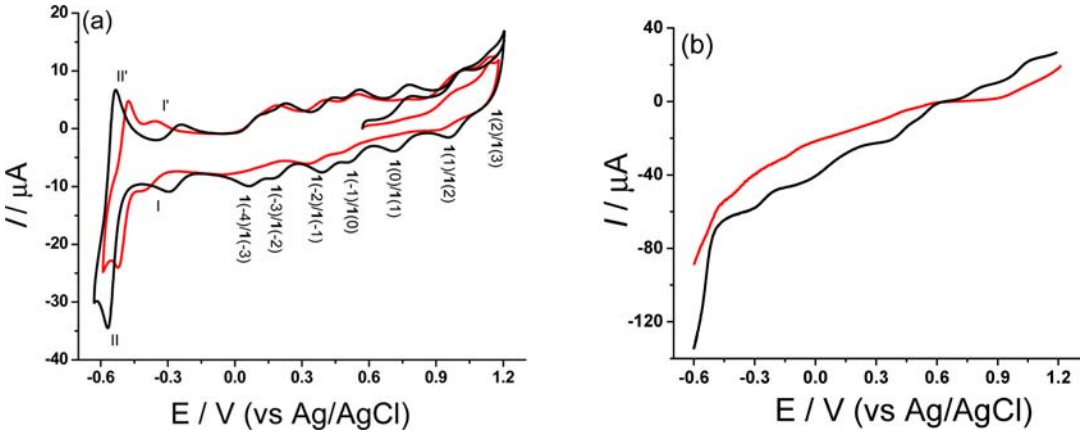

Figure 3. Voltammograms of 0.5 mM $[1(\gamma\text{-}SiW_{10}O_{36})_2]^{10-}$ in BR buffer (pH 2) in the presence (black trace) and absence (red trace) of 1 M KNO_3 at a 3 mm diameter glassy carbon electrode under (a) stationary (scan rate = 0.05 V s^{-1}) and (b) rotated disk electrode conditions (rotation rate = 104.7 rad s^{-1} and scan rate = 0.01 V s^{-1}).

dx.doi.org/10.1021/ic401748y | Inorg. Chem. 2013, 52, 11986−11996

Table 1. Reversible Potential, $E^{0'}$, and Peak Separation, ΔE_p, Values Derived from Cyclic Voltammograms Obtained from 0.5 mM $[\mathbf{1}(\gamma\text{-SiW}_{10}O_{36})_2]^{10-}$ in BR Buffer (pH 2) in the Presence of 1 M KNO_3[a]

process	**1**(1)/**1**(2)	**1**(0)/**1**(1)	**1**(−1)/**1**(0)	**1**(−2)/**1**(−1)	**1**(−3)/**1**(−2)	**1**(−4)/**1**(−3)	I/I′	II/II′
$E^{0'}$ (V)	1.003	0.763	0.529	0.429	0.218	0.096	−0.253	−0.538
ΔE_p (mV)	62.7	77.7	61.8	62.7	63.3	66.8	60.1	35.5

[a]Experimental conditions are as in the caption to Figure 3a.

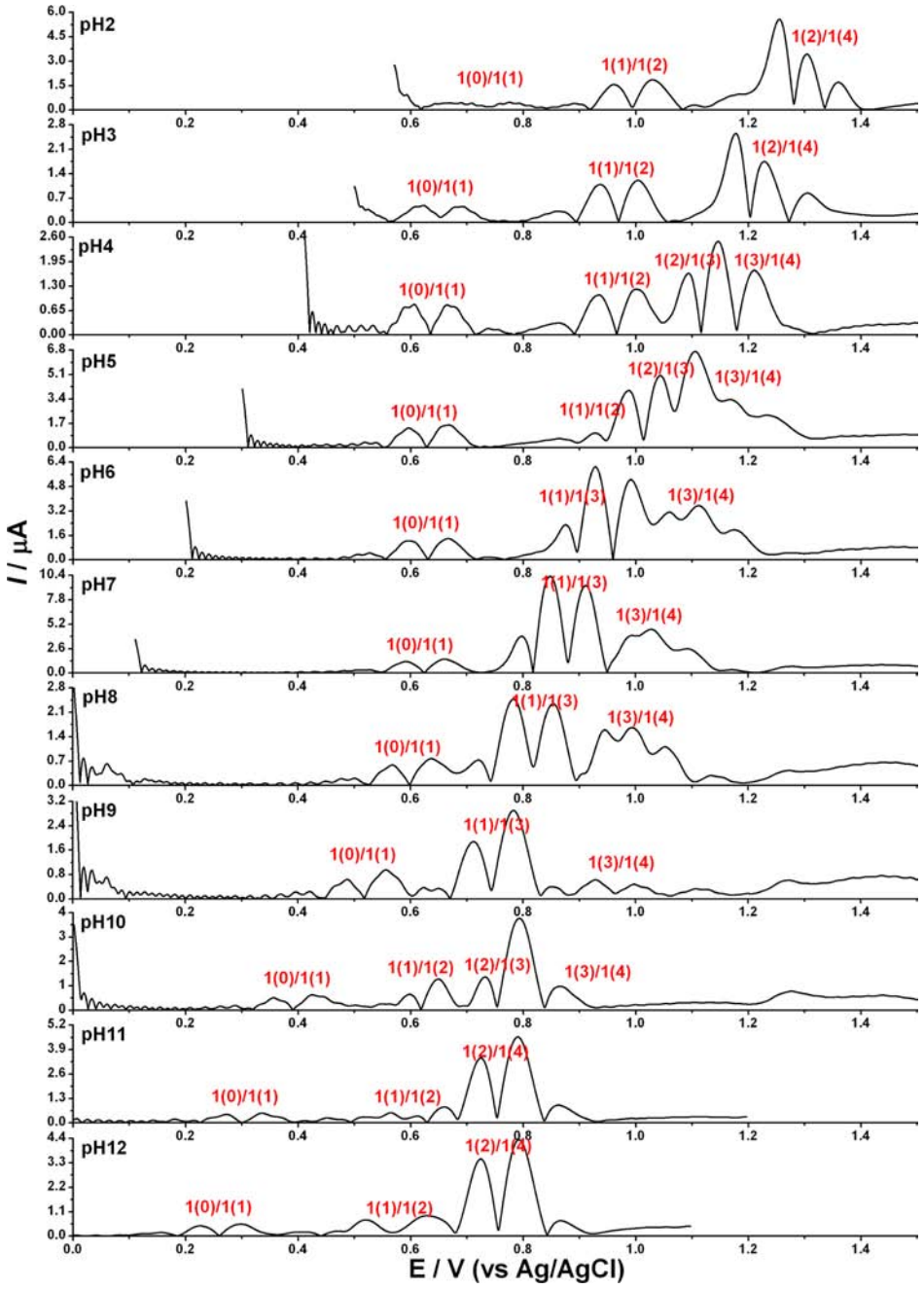

Figure 4. Fourth harmonic components of FTAC voltammogram at a 3 mm diameter GC electrode for 0.5 mM $[\mathbf{1}(\gamma\text{-SiW}_{10}O_{36})_2]^{10-}$ in BR buffer (pH = 2−12) in the presence of 1 M KNO_3: f = 9.02 Hz; ΔE = 0.08 V; ν = 0.0605 V s^{-1}.

Since the six processes associated with the Ru^{IV} centers occur over a narrow potential region, transient cyclic voltammetry is not an ideal method for assigning the redox level. To reliably decide whether the processes involve oxidation or reduction, steady-state RDE voltammograms for $[\mathbf{1}(\gamma\text{-SiW}_{10}O_{36})_2]^{10-}$ were obtained (Figure 3b). All oxidation (those with positive steady-state mass transport limiting current) processes and reduction (those showing a negative steady-state mass transport limiting current) are well-defined only when 1 M KNO_3 is present. RDE voltammograms in Figure 3b confirm that the assignments given above are correct. The reversible potential ($E^{0'}$) data derived from the half-wave ($E_{1/2}$) potentials of RDE voltammograms are similar to those obtained from midpoint

dx.doi.org/10.1021/ic401748y | Inorg. Chem. 2013, 52, 11986−11996

potentials with cyclic voltammetry (Table 1), which is as expected if reactions are reversible.

At pH 7, only the first oxidation process is reasonably well-defined when the ionic strength is low (Figure S2, Supporting Information) and characteristics of the voltammetry are electrode material dependent (Figure S3, Supporting Information), suggesting that the Frumkin effects are even more severe at neutral pH (more negatively charged) conditions. This may be explained using eq 5. POMs are negatively charged. Thus, K_3 which is associated with the more reduced form, may be assumed to be larger than K_4 (oxidized component) since this more highly charged reduced form should be a stronger base and hence a weaker acid. Thus, from eq 5, $k_{app}^{0'} \approx k_3^{0'}$ when $[H^+] \gg K_3$; $k_{app}^{0'} \approx k_1^{0'}$ when $[H^+] \ll K_4$. $k_1^{0'}$ is often lower than $k_3^{0'}$ for a POM,[25] and if this applies in the present case, the overall process will be less reversible at higher pH and therefore potentially more prone to influence from the Frumkin effect. When a high concentration of KNO_3 is added, the Frumkin effects are suppressed and cyclic voltammograms again become better defined (Figure S2, Supporting Information). Analogously, when the solution pH is in the region where $K_4 \ll [H^+] \ll K_3$, $k_{app}^{0'} \approx k_1^{0'}(K_4/[H^+])^{\alpha} + k_3^{0'}([H^+]/K_3)^{1-\alpha} \ll k_3^{0'}$. Under these slightly acidic conditions, the voltammetric processes for $[\mathbf{1}(\gamma\text{-}SiW_{10}O_{36})_2]^{10-}$ are also not as well-defined as found in this and previous work.[27]

FTAC Voltammograms for Oxidation of 1(0) in BR Buffer Containing KNO_3 as Additional Supporting Electrolyte. To explore the mechanism of catalytic oxygen evolution, it is crucial to know the reversible potentials of the $Ru^{IV/V}$ processes under catalytic turnover conditions. This information cannot be readily obtained using dc cyclic voltammetry under conditions of catalytic oxygen evolution reaction, especially when the underlying electron transfer processes are not reversible or the activity of the catalyst is high. In the present case, the catalytic current does not reach the ideal plateau predicted theoretically (sigmoidal shaped curve expected) due to the effect of the uncompensated ohmic IR_u drop (resulting from the high catalytic current) and a large contribution from background processes in the highly positive potential region where water is oxidized, making it impossible to accurately estimate the half-wave potential needed for a detailed theoretical analysis. In contrast, large amplitude FTAC voltammetry may allow the reversible potential to be measured directly, since the background rejected higher harmonic components are sensitive to the fast heterogeneous electron transfer process but insensitive to the catalytic water oxidation process.[40,41] This is because the ac waveform, superimposed onto the dc ramp, only probes the region of the diffusion layer near the electrode surface, which effectively remains unperturbed by the catalytic process.[40] FTAC voltammetry is also highly insensitive to sluggish background Faradaic processes,[42] which arise from the electrochemical instability of solvent, electrolyte, or electrode and which are likely to occur in the highly positive potential region where water is oxidized. In the FTAC method, reversible potentials can be conveniently taken as the average of the valley potentials from forward and reverse scans of potential in the case of even harmonic components and the average of the peak potentials from both forward and reverse scans in the case of odd harmonic components. This ac technique was used in our previous study to obtain the reversible potentials of $Ru^{IV/V}$ processes in acidic media that cannot be detected by dc cyclic voltammetry.[27] In this study, FTAC voltammetry is now used to obtain the reversible potentials of these $Ru^{IV/V}$ processes under a wide range of conditions to investigate the effect of both proton and electrolyte cations on the reversible potential of these processes.

Well-defined FTAC voltammograms with an amplitude, ΔE, of 80 mV and frequency, f, close to 9 Hz obtained in BR buffer media containing 1 M KNO_3 are shown in Figure 4 (4th harmonic only) and Figures S4 and S5 (5th and 6th harmonics), Supporting Information. When pH $\leq$ 4, processes $\mathbf{1}(2)/\mathbf{1}(3)$ and $\mathbf{1}(3)/\mathbf{1}(4)$ overlap, resulting in an overall two-electron transfer process, $\mathbf{1}(2)/\mathbf{1}(4)$. Electron transfer processes that result in the formation of $\mathbf{1}(4)$ from $\mathbf{1}(0)$ are shown in eqs 6–8 (coupled proton transfer processes and catalytic reactions are omitted for simplicity),

Process $\mathbf{1}(0)/\mathbf{1}(1)$:

$$\mathbf{1}(0) \rightleftharpoons \mathbf{1}(1) + e^- \quad (6)$$

Process $\mathbf{1}(1)/\mathbf{1}(2)$:

$$\mathbf{1}(1) \rightleftharpoons \mathbf{1}(2) + e^- \quad (7)$$

Process $\mathbf{1}(2)/\mathbf{1}(4)$:

$$\mathbf{1}(2) \rightleftharpoons \mathbf{1}(4) + 2e^- \quad (8)$$

This two-electron transfer process (Process $\mathbf{1}(2)/\mathbf{1}(4)$, eq 8) splits into two well-separated one-electron transfer processes ($\mathbf{1}(2)/\mathbf{1}(3)$ and $\mathbf{1}(3)/\mathbf{1}(4)$) at pH 5 as described by eqs 9 and 10. Under this pH condition, four well-defined one-electron transfer processes were detected.

Process $\mathbf{1}(2)/\mathbf{1}(3)$:

$$\mathbf{1}(2) \rightleftharpoons \mathbf{1}(3) + e^- \quad (9)$$

Process $\mathbf{1}(3)/\mathbf{1}(4)$:

$$\mathbf{1}(3) \rightleftharpoons \mathbf{1}(4) + e^- \quad (10)$$

When 6 $\leq$ pH $\leq$ 9, processes $\mathbf{1}(1)/\mathbf{1}(2)$ and $\mathbf{1}(2)/\mathbf{1}(3)$ merge into a single two-electron transfer process (process $\mathbf{1}(1)/\mathbf{1}(3)$, eq 11) and a one-electron transfer process $\mathbf{1}(3)/\mathbf{1}(4)$ now emerges.

Process $\mathbf{1}(1)/\mathbf{1}(3)$:

$$\mathbf{1}(1) \rightleftharpoons \mathbf{1}(3) + 2e^- \quad (11)$$

Process $\mathbf{1}(1)/\mathbf{1}(3)$ splits at pH 10, where process $\mathbf{1}(2)/\mathbf{1}(3)$ merges with process $\mathbf{1}(3)/\mathbf{1}(4)$ to form a two-electron transfer process, $\mathbf{1}(2)/\mathbf{1}(4)$. Analogous characteristics were also observed during the reduction of $\mathbf{1}(0)$ to $\mathbf{1}(-4)$. Both merging and splitting of redox processes occur under different pH and electrolyte conditions since the oxidized and reduced forms of $\mathbf{1}$ have different levels of interaction with protons and electrolyte cations, resulting in variable pH and electrolyte dependent characteristics as predicted theoretically (Figure 2 and Figure S1, Supporting Information).

Effects of Protons and Electrolyte Cations on the Reversible Potentials of Processes Involving Ru Centers. The reversible potentials of the processes involving the Ru centers in BR buffer solutions (pH 2–12) containing 1 M KNO_3 obtained from dc cyclic (midpoint potentials), RDE (half-wave potentials), and FTAC (peak (odd harmonics)/valley (even harmonics) potentials) voltammetry are summarized in Figure 5.

In an endeavor to establish whether there is a medium dependent contribution of junction potentials[31] in the

dx.doi.org/10.1021/ic401748y | Inorg. Chem. 2013, 52, 11986–11996

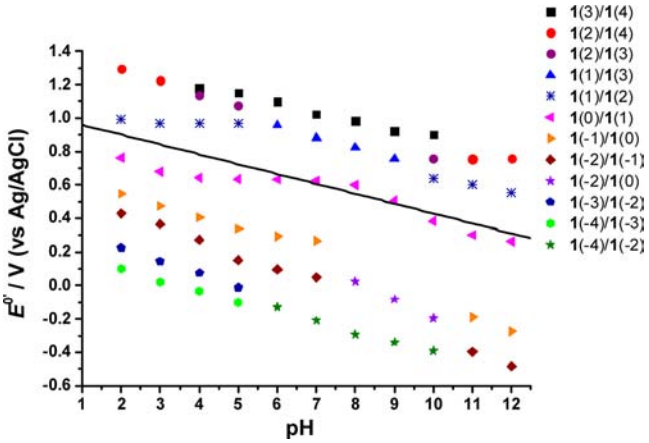

Figure 5. Dependence of the reversible potential ($E^{0'}$) on pH for one- and unresolved two-electron transfer processes. Data obtained in BR buffer solutions containing 0.5 mM $[\mathbf{1}(\gamma\text{-}SiW_{10}O_{36})_2]^{10-}$ and 1 M KNO_3 by dc cyclic, RDE, and FTAC voltammetry under conditions defined in the captions to Figures 3 and 4. The solid line represents the pH dependence of the reversible potential for the water oxidation process.

voltammetry of $\mathbf{1}(0)$, reversible potentials derived from the one-electron oxidation of 0.5 mM ferrocenemethanol (FcMeOH) to $FcMeOH^+$ were measured over the same pH conditions in the presence and absence of 1 M KNO_3. Since reversible potential data for the FcMeOH oxidation process were almost independent of the medium, it was assumed that variation of junction potential with pH and electrolyte variation is minimal.

The reversible potential data in Figure 5 exhibit a range of pH dependencies implying some variation in equilibrium constants associated with the different redox levels as deduced from the theoretical results displayed in Figure 2 and Figure S1, Supporting Information. In pH ranges where the reversible potentials are linearly dependent on pH with slopes close to 59 mV/pH, it is likely that equal numbers of protons and electrons are transferred in the reaction (in this case one proton, one electron). The pH dependent reversible potentials ($E^{0'}$ = 1.019−0.059 pH vs Ag/AgCl)[31] for water oxidation $2H_2O \rightarrow O_2 + 4H^+ + 4e^-$, are also included in Figure 5. Comparison of the two data sets enables the driving force of $\mathbf{1}(4)$ to be estimated for the overall four-electron proton coupled reaction described in eq 12,

$$\mathbf{1}(4) + 2H_2O \rightarrow \mathbf{1}(0) + O_2 + 4H^+ \quad (12)$$

The data in Figure 5 reveal the following: (a) The reaction in eq 12 is thermodynamically favored over the whole pH range examined, given the negative Gibbs free energy change ($\Delta G = -nF\Delta E^{0'}$) for this reaction; this conclusion is based on the apparent reversible potential of the $\mathbf{1}(4)/\mathbf{1}(0)$ process ($E^{0'}_{app}$), which involves multiple electron transfer steps and was determined using Hess' law.[43] If all steps involve one-electron, $E^{0'}_{app}$ is the average of the reversible potentials of all steps. The water oxidation reaction in eq 12 is represented as a commonly accepted concerted proton coupled four-electron transfer process.[20,22] The formation of other intermediates by one-, two-, or three-electron transfer pathways is thermodynamically unfavorable even if the $\mathbf{1}(4)/\mathbf{1}(3)$ redox couple (with the most positive reversible potential) is involved.[20,22,44] The probability of achieving water oxidation via four simultaneous $\mathbf{1}(4)/\mathbf{1}(3)$ one-electron transfer processes to generate oxygen would involve six molecules; thus though thermodynamically favorable, it is statistically unlikely. (b) When the pH is in the range of 2−8, the reversible potential of at least one oxidation process can be pH independent, suggesting that proton transfer need not necessarily be coupled to all electron transfer steps during water oxidation by $\mathbf{1}(4)$. (c) Even though the reversible potential for the water oxidation process shifts 59 mV per pH to more negative values when the pH increases, the driving force for water oxidation by $\mathbf{1}(4)$ does not necessarily increase since the reversible potentials associated with this and other oxidation reactions also shift in the negative potential direction.

pH dependent shifts in $E^{0'}$ also were obtained when 10 mM $Ca(NO_3)_2$ (lower concentration was used due to lower solubility of Ca^{2+} salts in neutral and basic pH buffers) or 1 M $NaNO_3$, $LiNO_3$, $Mg(NO_3)_2$, $MgSO_4$, or Na_2SO_4 instead of 1 M KNO_3. In the 10 mM $Ca(NO_3)_2$, 1 M $Mg(NO_3)_2$, or 1 M $MgSO_4$ cases, data are only available for pH ≤ 8 due to limited solubility of the salts in alkaline conditions. The FTAC voltammograms of the oxidation processes are less well-defined in these electrolytes (4th−6th harmonics, Figures S6−S23, Supporting Information) than in 1 M KNO_3 (Figure 4 and Figures S4 and S5, Supporting Information). This makes it difficult to precisely determine reversible potentials so only the values for the reduction processes are displayed in Figures S24−S29, Supporting Information. These reduction processes also vary with pH, again with a slope of ∼59 mV/pH in several pH regions. For these cases, the dependence is not strongly dependent on the identity of the electrolyte. Clearly, interaction with K^+ is the strongest.

Consideration of *K* Values Associated with Process 1(0)/1(1). Quantitative deduction of K values for all redox levels, given the series of assumptions associated with theoretical description given for the simplest case above, is problematic. However, process $\mathbf{1}(0)/\mathbf{1}(1)$ meets most of the requirements, so it is considered in some detail. The dc cyclic voltammetric responses for this first oxidation process are always well-defined, essentially reversible, and well separated from neighboring processes irrespective of electrolyte. The reversible potentials for this process obtained as a function of pH in the presence of different added electrolytes are summarized in Figure 6. The results establish that in the presence of 1 M KNO_3, the $E^{0'}$−pH relationship is distinctly different from that found when 1 M $LiNO_3$, $NaNO_3$, Na_2SO_4, $Mg(NO_3)_2$, or $MgSO_4$ or 10 mM $Ca(NO_3)_2$ is present. Thus, the transition point where the $E^{0'}$−pH curve becomes less dependent on pH in the presence of 1 M KNO_3 occurs at much lower pH, suggesting that the interaction between K^+ and $\mathbf{1}(0)$ is stronger.

Since the pH dependence of the reversible potential of the $\mathbf{1}(0)$ process is essentially independent of the identity of the added electrolyte other than KNO_3, it may be assumed that these cations are relatively innocent over the entire pH range examined. This assumption allows quantitative analysis of some of the equilibrium constant data under neutral to acid conditions to be undertaken using the theory presented above. Thus, it can be noted that Figure 6 contains a plateau region. Access to this region is a key feature needed to interpret data and occurs over the acidic pH range of about 4 to 6.5 in the absence of K^+ and about 6 to 8 in the presence of this cation. Furthermore, and again as necessary to apply the theory, the very low pH region of 2 to 4 has a slope of close to 59 mV per change in pH unit implying a one proton, one electron

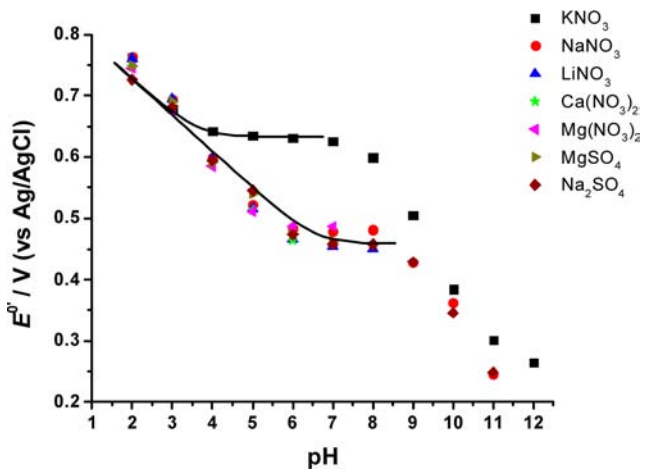

Figure 6. Dependence of the reversible potential ($E^{0'}$) on pH for the one-electron oxidation process $\mathbf{1}(0)/\mathbf{1}(1)$. Data obtained in BR buffer solutions containing 0.5 mM $[\mathbf{1}(\gamma\text{-}SiW_{10}O_{36})_2]^{10-}$ and 1 M KNO_3, $NaNO_3$, or $LiNO_3$, 10 mM of $Ca(NO_3)_2$, or 1 M $Mg(NO_3)_2$, $MgSO_4$, or Na_2SO_4. The solid black curves represent the best fit to the theoretical relationship computed using $pK_3 \leq 1$, $pK_4 = 6.55$, and $E_1^{0'} = 0.458$ V for the lower plot and these parameters along with $pK_1 \leq 0$ and $pK_2 = 2.96$ for the upper plot. Other parameters as well as assumptions used in the calculations are described in the text.

change is associated with process $\mathbf{1}(0)/\mathbf{1}(1)$ in the absence KNO_3. However, in the presence of 1 M KNO_3, while the very low pH region is the same as in the absence of potassium cation, there is a pH region of about 4 to 7 that has the reversible potential versus pH slope characteristics derived from a one potassium ion, one electron $\mathbf{1}(0)/\mathbf{1}(1)$ process, that should be amendable to modeling as per Scheme 1.

Before proceeding to describe the results of modeling the proton and potassium cation dependence in the acid region, it has to be pointed out that there is major difficulty in establishing the chemical identities of species designated as A and B in the general theory. While the symbolism used of $[\mathbf{1}(\gamma\text{-}SiW_{10}O_{36})_2]^{10-}$ in this and other papers is valid for the solid state structure, a species with a 10 minus charge is very unlikely to exist in solution at any pH. Thus, protonation of $[\mathbf{1}(\gamma\text{-}SiW_{10}O_{36})_2]^{10-}$ and the oxidized analogue, $[\mathbf{1}(\gamma\text{-}SiW_{10}O_{36})_2]^{9-}$, is likely to occur even under alkaline conditions to lower the charge. The reversible potential data in pH region 8−12 in Figure 6 for process $\mathbf{1}(0)/\mathbf{1}(1)$, despite being derived from a Ru oxidation reaction, are therefore assumed to reflect protonation changes associated predominantly with the W framework, noting that reduction processes I/I′ and II/II′ designated as being framework based ones are highly sensitive to pH. Nevertheless, the fact that a plateau is obtained at lower pH over range 4 to 7.5 implies that both redox levels have the same formulation over this pH range.

Modeling of the acid region according to Scheme 1 was therefore undertaken as follows, noting that since the processes are reversible, terms associated with electrode kinetics can be ignored. In the protocol adopted, the $E^{0'}$−pH curves for all non-KNO_3 electrolyte cases were first compared with the theoretical predictions (only the effects of proton were considered) to obtain the values of pK_3 for A, pK_4 for B and $E_1^{0'}$ for process A/B. On this basis, values of $pK_3 \leq 1$, $pK_4 = 6.55$, and $E_1^{0'} = 0.458$ V were obtained by least-squares fitting of the experimental data to the theory. Subsequent use of these predetermined and now assumed to be known values facilitates determination of pK_1 for A and pK_2 for B of the noninnocent ion, K^+, by comparison of experimental data with the theoretical data calculated on the basis of eq 1. In this manner, values of $pK_1 \leq 0$ and $pK_2 = 2.96$ were obtained using least-squares fittings, which implies that the interaction of **1** with K^+, though significant, is much weaker than protonation. Here it is worth mentioning, that the pH titration of $\mathbf{1}(0)$ in the absence of electrolytes revealed that there are two pK's with estimated values around 3−4.[7] Clearly, as suggested by this study, both ionic strength of the reaction medium and the identity of the electrolyte have pronounced effects on the acid−base properties of POMs. Further investigations of acid−base properties of **1** at high ionic strength are in progress.

The fact that the potassium cation appears to be selectively significant in terms of oxidation of the ruthenium $\mathbf{1}(0)$ center is plausibly due to an electrostatic effect. The hydrodynamic radius of K^+ is the smallest among the cations studied as judged by its largest diffusion coefficient[44] and in accordance with the Stokes−Einstein law.[43] The hydrodynamic radii of Mg^{2+} and Ca^{2+} are about 2−3 fold that of K^+.[44] Therefore, one may expect both Mg^{2+} and Ca^{2+} have weaker electrostatic interactions with $\mathbf{1}(0)$ in comparison with K^+, even though they have a higher charge. A specific binding interaction of **1** with K^+ is also plausible, likely due to the ability of K^+ to compete with proton for the same oxygen site in the Ru_4 core, but more studies on the origin of this cation interaction, using other techniques, are needed to provide a definitive account of the nature of this interaction.

It should also be noted that even though the $E^{0'}$−pH data for process $\mathbf{1}(0)/\mathbf{1}(1)$ is different in the presence of K^+, the reversible potentials for the other three oxidation processes are not as strongly dependent on the identity of the cation (Figure 4 and Figures S4−S23, Supporting Information). As a result, electrochemically generated $\mathbf{1}(4)$ is always strong enough to oxidize water (eq 12) in all electrolyte media.

Identifying Catalytically Active Forms of 1(0) as a Function of pH in the Presence of 1 M KNO_3. The reversible potential data in Figure 5 and Figures S6−S23, Supporting Information, suggest that sufficiently oxidized forms of $\mathbf{1}(0)$ are capable of catalyzing water oxidation. The RRDE method may be used to assist in the identification of the catalytically active forms of **1**.[31]

During RRDE measurements, a dc ramped potential was applied to the disk electrode at a scan rate of 20 mV s^{-1}. A suitable potential was applied to the ring electrode to detect O_2 formation under mass transport controlled conditions after it was swept to the ring electrode, following generation in the region close to the GC disk electrode. When the catalytic activity of the catalyst is not very high, as in the present case, the disk current is a function of the rotation rate and thus is affected by hydrodynamic mass transport. As a result, electroactive unreacted catalyst can be detected at the ring. In these circumstances, quantitative analysis of data to obtain the TOF of the catalyst requires a numerical simulation that takes into account contributions from both homogeneous and heterogeneous electron transfer processes under convective-diffusion conditions. This represents a daunting task. However, qualitatively informative information can be readily obtained from RRDE data under circumstances relevant to this study that still provides valuable information on the relative activity of $\mathbf{1}(0)$ in each redox level as reported below.

RRDE measurements were undertaken at pH 2, 4, 5, 6, 8, 10, and 12 in the presence of 1 M KNO_3. The initial potential of

dx.doi.org/10.1021/ic401748y | Inorg. Chem. 2013, 52, 11986−11996

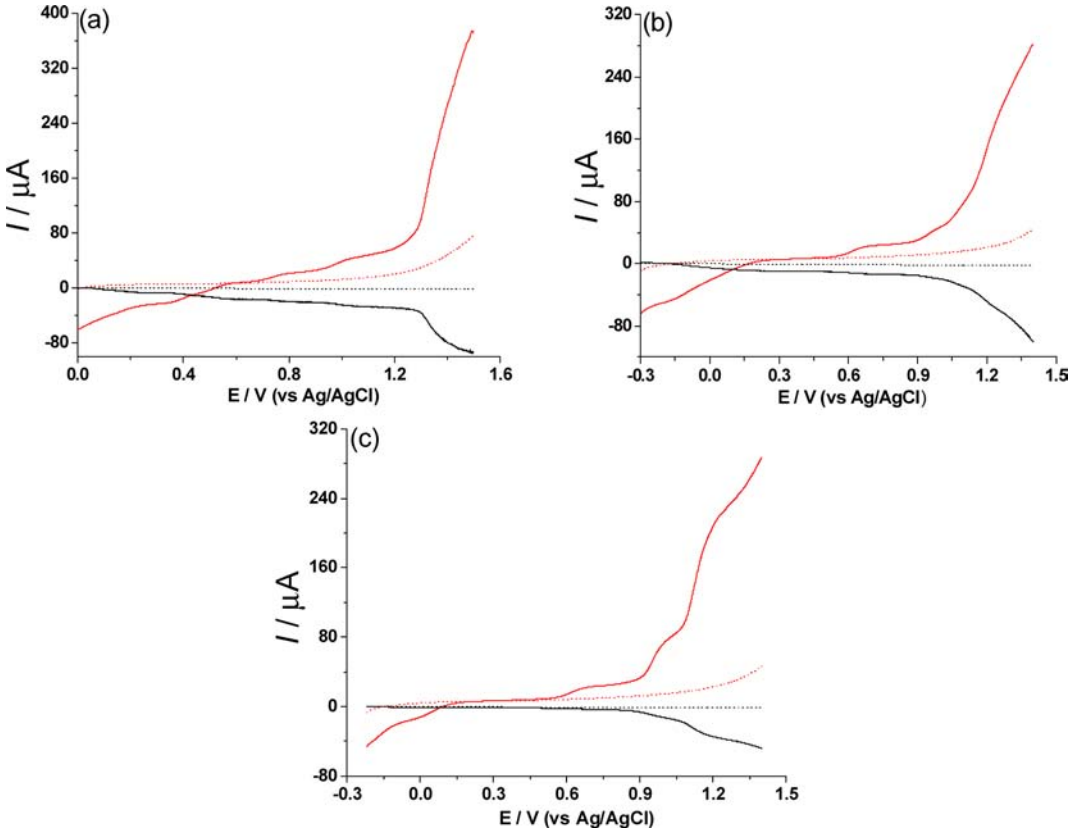

Figure 7. RRDE voltammograms (red traces, disk response; black traces, ring response) obtained in BR buffer solutions at (a) pH 2, (b) pH 5, and (c) pH 6 in the absence of (dotted traces) or presence of 0.5 mM (solid traces) $[\mathbf{1}(\gamma\text{-}SiW_{10}O_{36})_2]^{10-}$ and 1 M KNO_3. The potential of the disk electrode was swept in the positive direction at a scan rate of 20 mV s^{-1} while a constant potential equal to the initial potential at the disk electrode was applied to the ring electrode in order to monitor the formation of O_2 generated at the disk electrode. Rotation rate: 104.7 rad s^{-1}.

the disk electrode was set at the same value as that applied at the ring electrode. Results at pH 2, 5, and 6 are summarized in Figure 7. If the current at the ring electrode at the initial potential is set to be zero for convenience to remove contributions from unreacted catalyst, then the negative current at ring electrode approximately indicates the detection of the electroactive oxygen generated at the disk electrode.

At pH $\leq$ 4 (Figure 7a, Figure S24a, Supporting Information), the results are relatively simple to understand. The steady-state mass transport limiting currents for the two initial one-electron oxidation processes are as expected if **1**(1) and **1**(2) are not catalytically active at this pH. In contrast, the current at the disk electrodes, when the combined two-electron oxidation process **1**(2)/**1**(4) occurs and **1**(4) forms, is greatly enhanced due to the catalytic oxidation of water (eq 12). This results in formation of reducible and ring detectable O_2, as reported in our earlier studies.[19] If the increase in disk current in these experiments was due to the catalytic oxidation of an electroinactive species, then a decrease in ring current is expected: electrogenerated **1**(4) would then be consumed without leading to the formation of a ring detectable species. Consequently, it is important to always monitor the ring current. The fact that enhanced current was observed at both the ring and disk electrodes confirms that **1** is an active water oxidation catalyst. Otherwise, catalytic current would not have been detected under the hydrodynamic conditions associated with the RRDE, where the contribution from homogeneous catalysis to voltammetric response, relative to the stationary electrode condition, is suppressed due to the greatly enhanced mass transport rate.[31]

At pH 5 (Figure 7b), **1**(1) and **1**(2) remain catalytically inactive, but both **1**(3) and **1**(4) are active with the latter being more active as judged from the magnitudes of the ring and disk currents. These results are expected since both **1**(3) and **1**(4) are thermodynamically capable of oxidizing water via the most efficient four-electron transfer pathway based on the data shown in Figure 5.

At pH 6 and 8 (Figure 7c and Figure S24b, Supporting Information), **1**(1) remains catalytically inactive (the steady-state mass transport limiting currents for this one-electron oxidation process and the one-electron reduction process are equal). However, **1**(3) generated in the second overall two-electron oxidation process is catalytically active (reduction currents detected at both ring and disk electrodes are clearly more than twice that of the first one-electron oxidation process), although the activity is much lower than that of **1**(4). Again, this is completely consistent with the thermodynamic considerations described above. The results at pH 10 (Figure S24c, Supporting Information) are similar to those obtained at pH 5 in the sense that **1**(1) and **1**(2) remain catalytically inactive and **1**(3) and **1**(4) active. In this case, if **1**(3) undergoes the most efficient four-electron transfer pathway to generate O_2, it could be concluded that there will be a shortage of ~30 mV in driving force based on the data shown in Figure 5. However, this deficiency lies within the uncertainty associated with comparing the theoretical oxygen potential dependence on pH and the reversible potential measurement.

dx.doi.org/10.1021/ic401748y | *Inorg. Chem.* 2013, 52, 11986−11996

At pH 12 (Figure S24d, Supporting Information), **1**(1) remains inactive, but it is very difficult from the RRDE response to determine whether **1**(2) is now active, since this process is very close to that for the subsequent overall two-electron oxidation process, which leads to formation of highly active **1**(4).

CONCLUSIONS

A detailed investigation of the rich redox chemistry of $[\mathbf{1}(\gamma\text{-}SiW_{10}O_{36})_2]^{10-}$ in aqueous media has been undertaken over wide pH and ionic strength ranges using BR buffer media containing a variety of added supporting electrolytes and employing dc cyclic, rotating disk electrode, and large amplitude Fourier transformed alternating current voltammetric techniques. The results reveal that well-defined voltammograms can be obtained over the pH range of 2−12 provided Frumkin double layer effects are suppressed by addition of adequate concentrations of supporting electrolyte over that provided by the buffer alone. Detailed analysis of the pH dependence of reversible potentials associated with the **1**(0)/**1**(1) process suggests that (a) K^+ interacts more strongly with **1**(1) than do Li^+, Na^+, Mg^{2+}, or Ca^{2+}, (b) proton transfer may not necessarily be coupled to all electron transfer steps that generate water oxidizing intermediate forms of **1**, (c) the four-electron oxidized form, **1**(4), is capable of oxidizing water under all conditions studied, and (d) the three-electron oxidized form, **1**(3), also may exhibit considerable water oxidation catalytic activity.

ASSOCIATED CONTENT

Supporting Information

Theoretical results on the dependence of $(E^{0'}_{app} - E^{0'}_1)$ on (pH − pK_4) as a function of (pM − pK_2) calculated from eq 1 for (a) $pK_2 - pK_1 = 0$ and $pK_4 - pK_3 = 5$, effect of the ionic strength and electrode material on dc cyclic voltammetry of **1**, FTAC voltammetry of **1** in different electrolyte media, dependence of the reversible potential $E^{0'}$ on pH for the well-defined reduction processes associated with **1** in different electrolyte media with high ionic strength, and RRDE voltammograms of $[\mathbf{1}(\gamma\text{-}SiW_{10}O_{36})_2]^{10-}$ obtained in BR buffer solutions at different pH values in the presence of 1 M KNO_3. This material is available free of charge via the Internet at http://pubs.acs.org.

AUTHOR INFORMATION

Corresponding Authors

*E-mail: alan.bond@monash.edu.
*E-mail: jie.zhang@monash.edu.
*E-mail: iguelet@emory.edu.

Notes

The authors declare no competing financial interest.

ACKNOWLEDGMENTS

The authors gratefully acknowledge financial support from the Australian Research Council and from the U.S. National Science Foundation Grant CHE-0911610, and valuable discussions with Dr. Stephen Feldberg (Brookhaven National Laboratory, USA).

REFERENCES

(1) Pope, M. T. *Heteropoly and Isopoly Oxometalates*; Springer-Verlag: Berlin, 1983.
(2) Hill, C. L. *Chem. Rev.* **1998**, *98*, 1.
(3) Sadakane, M.; Steckhan, E. *Chem. Rev.* **1998**, *98*, 219.
(4) Keita, B.; Nadjo, L. *J. Mol. Catal. A: Chem.* **2007**, *262*, 190.
(5) Sartorel, A.; Carraro, M.; Scorrano, G.; Zorzi, R. D.; Geremia, S.; McDaniel, N. D.; Bernhard, S.; Bonchio, M. *J. Am. Chem. Soc.* **2008**, *130*, 5006.
(6) Costentin, C.; Robert, M.; Saveant, J.-M. *Chem. Rev.* **2010**, *110*, PR1.
(7) Geletii, Y. V.; Botar, B.; Kögerler, P.; Hillesheim, D. A.; Musaev, D. G.; Hill, C. L. *Angew. Chem., Int. Ed.* **2008**, *47*, 3896.
(8) Yin, Q.; Tan, J. M.; Besson, C.; Geletii, Y. V.; Musaev, D. G.; Kuznetsov, A. E.; Luo, Z.; Hardcastle, K. I.; Hill, C. L. *Science* **2010**, *328*, 342.
(9) Murakami, M.; Hong, D.; Suenobu, T.; Yamaguchi, S.; Ogura, T.; Fukuzumi, S. *J. Am. Chem. Soc.* **2011**, *133*, 11605.
(10) Bernardini, G.; Zhao, C.; Wedd, A. G.; Bond, A. M. *Inorg. Chem.* **2011**, *50*, 5899.
(11) Howells, A. R.; Sankarraj, A.; Shannon, C. *J. Am. Chem. Soc.* **2004**, *126*, 12258.
(12) Stracke, J. J.; Finke, R. G. *J. Am. Chem. Soc.* **2011**, *133*, 14872.
(13) Zhu, G. B.; Geletii, Y. V.; Kogerler, P.; Schilder, H.; Song, J.; Lense, S.; Zhao, C. C.; Hardcastle, K. I.; Musaev, D. G.; Hill, C. L. *Dalton Trans.* **2012**, *41*, 2084.
(14) Stracke, J. J.; Finke, R. G. *ACS Catal.* **2013**, *3*, 1209.
(15) Geletii, Y. V.; Besson, C.; Hou, Y.; Yin, Q.; Musaev, D. G.; Quinonero, D.; Cao, R.; Hardcastle, K. I.; Proust, A.; Ko□gerler, P.; Hill, C. L. *J. Am. Chem. Soc.* **2009**, *131*, 17360.
(16) Natali, M.; Orlandi, M.; Berardi, S.; Campagna, S.; Bonchio, M.; Sartorel, A.; Scandola, F. *Inorg. Chem.* **2012**, *51*, 7324.
(17) Toma, F. M.; Sartorel, A.; Iurlo, M.; Carraro, M.; Parisse, P.; Maccato, C.; Rapino, S.; Gonzalez, B. R.; Amenitsch, H.; Da Ros, T.; Casalis, L.; Goldoni, A.; Marcaccio, M.; Scorrano, G.; Scoles, G.; Paolucci, F.; Prato, M.; Bonchio, M. *Nat. Chem.* **2010**, *2*, 826.
(18) Quintana, M.; Lopez, A. M.; Rapino, S.; Toma, F. M.; Iurlo, M.; Carraro, M.; Sartorel, A.; Maccato, C.; Ke, X. X.; Bittencourt, C.; Da Ros, T.; Van Tendeloo, G.; Marcaccio, M.; Paolucci, F.; Prato, M.; Bonchio, M. *ACS Nano* **2013**, *7*, 811.
(19) Guo, S.-X.; Liu, Y.; Lee, C.-Y.; Bond, A. M.; Zhang, J.; Geletii, Y. V.; Hill, C. L. *Energy Environ. Sci.* **2013**, *6*, 2654.
(20) Costentin, C.; Robert, M.; Saveant, J.-M. *Acc. Chem. Res.* **2010**, *43*, 1019.
(21) Weinberg, D. R.; Gagliardi, C. J.; Hull, J. F.; Murphy, C. F.; Kent, C. A.; Westlake, B. C.; Paul, A.; Ess, D. H.; McCafferty, D. G.; Meyer, T. J. *Chem. Rev.* **2012**, *112*, 4016.
(22) Huynh, M. H. V.; Meyer, T. J. *Chem. Rev.* **2007**, *107*, 5004.
(23) Piccinin, S.; Sartorel, A.; Aquilanti, G.; Goldoni, A.; Bonchio, M.; Fabris, S. *Proc. Natl. Acad. Sci. U. S. A.* **2013**, *110*, 4917.
(24) Bond, A. M. *Broadening Electrochemical Horizons*; Oxford Press: New York, 2002.
(25) Guo, S. X.; Feldberg, S. W.; Bond, A. M.; Callahan, D. L.; Richardt, P. J. S.; Wedd, A. G. *J. Phys. Chem. B* **2005**, *109*, 20641.
(26) Piccinin, S.; Fabris, S. *Phys. Chem. Chem. Phys.* **2011**, *13*, 7666.
(27) Lee, C.-Y.; Guo, S.-X.; Murphy, A. F.; McCormac, T.; Zhang, J.; Bond, A. M.; Zhu, G.; Hill, C. L.; Geletii, Y. V. *Inorg. Chem.* **2012**, *51*, 11521.
(28) Guo, S. X.; Mariotti, A. W. A.; Schlipf, C.; Bond, A. M.; Wedd, A. G. *Inorg. Chem.* **2006**, *45*, 8563.
(29) Zhang, J.; Goh, J. K.; Tan, W. T.; Bond, A. M. *Inorg. Chem.* **2006**, *45*, 3732.
(30) Geletii, Y. V.; Botar, B.; Kögerler, P.; Hillesheim, D. A.; Musaev, D. G.; Hill, C. L. *Angew. Chem.* **2008**, *120*, 3960.
(31) Bard, A. J.; Faulkner, L. R. *Electrochemical Methods: Fundamentals and Applications*, 2nd ed.; New York: John Wiley, 2001.
(32) Bond, A. M.; Coomber, D. C.; Feldberg, S. W.; Oldham, K. B.; Vu, T. *Anal. Chem.* **2001**, *73*, 352.
(33) Delahay, P. *Double Layer and Electrode Kinetics*; Wiley: New York, 1965.
(34) Bond, A. M. In *Trends in Molecular Electrochemistry*; Pombeiro, A. J. L., Amatore, C., Eds.; Marcel Dekker: New York, 2004; p 445.

(35) Bond, A. M.; Duffy, N. W.; Guo, S.-X.; Zhang, J.; Elton, D. *Anal. Chem.* **2005**, *77*, 186A.
(36) Britton, H. T. S.; Robinson, R. A. *J. Chem. Soc.* **1931**, 1456.
(37) Sawyer, D. T.; Sobkowiak, A.; Roberts, J., J.L. *Electrochemistry for Chemists*, 2nd ed.; Wiley: New York, 1995.
(38) Heyrovský, J.; Kůta, J. *Principles of Polarography*; Academic Press: New York, 1966.
(39) Laviron, E. *J. Electroanal. Chem. Interfacial Electrochem.* **1981**, *124*, 1.
(40) Zhang, J.; Bond, A. M. *J. Electroanal. Chem.* **2007**, *600*, 23.
(41) Fleming, B. D.; Zhang, J.; Bond, A. M.; Bell, S. G.; Wong, L. L. *Anal. Chem.* **2005**, *77*, 3502.
(42) Zhang, J.; Guo, S. X.; Bond, A. M.; Marken, F. *Anal. Chem.* **2004**, *76*, 3619.
(43) Atkins, P.; De Paula, J. *Atkins' Physical Chemistry*, 8th ed.; Oxford University Press: Oxford, 2006.
(44) Mills, R.; Lobo, V. M. M. *Sel-diffusion in Electrolyte Solutions*; Elsevier: Amsterdam, 1989.